Macromolecules
ARTICLE

Macromolecules **2011**, *44*, 1125–1131 **1125**
DOI: 10.1021/ma101982u

Phase Behavior and Photoresponse of Azobenzene-Containing Polystyrene-*block*-poly(*n*-butyl methacrylate) Block Copolymers

Wei Chen,[†] Xinyu Wei,[†] Anna C. Balazs,[‡] Krzysztof Matyjaszewski,*[,§] and Thomas P. Russell*[,†]

[†]*Department of Polymer Science and Engineering, University of Massachusetts, Amherst, Massachusetts 01003, United States,* [‡]*Department of Chemical Engineering, University of Pittsburgh, Pittsburgh, Pennsylvania 15213, United States, and* [§]*Department of Chemistry, Carnegie Mellon University, Pittsburgh, Pennsylvania 15213, United States*

Received August 26, 2010; Revised Manuscript Received December 30, 2010

ABSTRACT: It is well-known that polystyrene-*block*-poly(*n*-butyl methacrylate) (PS-*b*-P*n*BMA) block copolymers (BCPs) exhibit an hourglass-shaped phase diagram, resulting from the simultaneous appearance of an upper order-to-disorder transition (UODT) and a lower disorder-to-order transition (LDOT). Here, the phase behavior of three azobenzene-containing PS-*b*-P*n*BMA BCPs was investigated by small-angle neutron scattering (SANS). As to their molecular weights of M_n = 24 000, 40 000, and 47 000, the three copolymers are designated as Azo24k, Azo40k, and Azo47k, respectively. Temperature-dependent SANS data show that Azo24k and Azo40k BCPs are closer to their corresponding LDOT and UODT, respectively, while Azo47k BCP locates in the middle of temperature interval between UODT and LDOT. This indicates that after incorporating azobenzene functionalities into P*n*BMA blocks, the azobenzene-containing PS-*b*-P*n*BMA BCPs still exhibit both LDOT and UODT, characteristic of the "compressibility" similar to their parent PS-*b*-P*n*BMA BCPs. After exposing the films of three azobenzene-containing PS-*b*-P*n*BMA BCPs to UV light with a wavelength of 365 nm, the photoisomerization of azobenzene produces light-induced motions and thereby gives rise to conformational increase and density variation, which can result in a significant increase in entropy. As a consequence, three disordered azobenzene-containing PS-*b*-P*n*BMA BCPs are driven toward LDOT.

Introduction

Design, synthesis, and engineering of photoresponsive polymers are emerging areas of scientific interest and unexplored commercial applications.[1−5] As photoisomerization of azobenzene is a clean and efficient reversible process, azobenzene-containing polymers have been the center of interest in exploring light-responsive polymers.[6−12] The azobenzene molecule isomerizes from a stable *trans* state to a metastable *cis* state upon UV irradiation, and the *cis* isomer is able to be switched back to the *trans* by visible light or heat. On the *trans*−*cis* conversion, azobenzene changes its molecular shape and the distance between the *para*-positions is reduced from 9 to 5.9 Å.[8] Consequently, when azobenzene is incorporated into a polymer, the photoisomerization can generate the motions ranging from slight reorientation of the chromophore to massive motion of the polymer materials.[12−14]

Block copolymers (BCPs), two or more polymers connected by a covalent bond at one end, self-assemble into a series of well-defined nanostructures.[15−21] Thus, the combination of the appealing features of azobenzene-containing polymers and BCPs is anticipated to lead to intriguing systems. Most recently, Seki, Iyoda, and Ikeda's research groups[11,22−24] have successfully controlled microphase separation and microdomain orientation in azobenzene-containing BCPs by linear polarized UV light, experimentally demonstrating that light could be utilized to tune the morphology of azobenzene-containing BCPs. Meanwhile, Balazs and co-workers have predicted that long-range ordering of BCP microdomains can be produced over a macroscopic scale by successively sweeping BCPs with a series of light bands. These light bands, in principle, would reversibly bring BCPs through an ordering transition from a homogeneous mixture to an ordered state with microdomains of each block, so that BCP microdomains could be epitaxially "crystallized" in the growing front.[25,26]

In a previous study, we have reported that the photocontrol over an ordering process from a disordered state could be achieved in azobenzene-containing polystyrene-*block*-poly(*n*-butyl methacrylate) (PS-*b*-P*n*BMA) BCP mixtures.[27,28] However, it is still challenging to tailor such an ordering process in a controllable and predictable fashion and hence requires comprehensive understanding on the interplay between photoactivity and microphase separation. In this article, we have investigated the phase behaviors and photoresponses of three deuterated polystyrene-*block*-poly(*n*-butyl methacrylate-*random*-2-(4-(phenylazo)benzoate)ethyl methacrylate) (d_8-PS-*b*-P(*n*BMA-*r*-AzoEMA)) BCPs with different molecular weights (MWs) and compositions by small-angle neutron scattering (SANS). It should be noted that in contrast to the classical, enthalpy-driven upper order-to-disorder transition (UODT), the parent PS-*b*-P*n*BMA BCPs microphase-separate upon heating, that is, a lower disorder-to-order transition (LDOT) that originates from an increase in entropy due to the disparities in compressibilities of two blocks.[29−47] After the integration of azobenzene functionalities into P*n*BMA blocks, all three d_8-PS-*b*-P(*n*BMA-*r*-AzoEMA) BCPs still maintain the "compressible" nature, but the phase behaviors become highly dependent on the temperature dependence of χ. Although the LDOT may also arise from directional interactions, PS and PnBMA are weakly interacting without special interactions, like hydrogen bonds and strong dipole−dipole interactions, especially at an elevated temperature higher than 130 °C. Moreover, for the P(*n*BMA-*r*-AzoEMA)

*To whom correspondence should be addressed. E-mail: russell@mail.pse.umass.edu.

Published on Web 02/03/2011

Scheme 1. Chemical Structure of d_8-PS-*b*-P(*n*BMA-*r*-AzoEMA) BCP and Its Associated Photoisomerization[a]

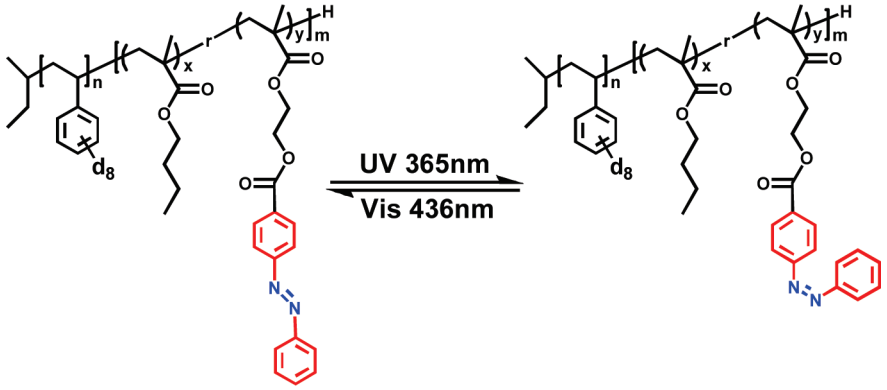

[a] Azobenzene chromophores isomerize from the stable *trans* state into the metastable *cis* state upon UV irradiation. The *cis* isomers then can either thermally relax back to the *trans* state or may be photoisomerized into that state by visible light.

Table 1. Characteristics of Three d_8-PS-*b*-P(*n*BMA-*r*-AzoEMA) Copolymers[a]

	M_n	M_w	PDI	d_8-PS:PAzoEMA:PnBMA (wt %)
Azo24k	24 000	25 000	1.04	58.3:16.7:25.0
Azo47k	47 200	52 000	1.07	51.9:24.8:23.3
Azo40k	40 000	42 000	1.05	64.5:13.0:22.5

[a] The weight fraction of d_8-PS was determined by GPC and the ratio of PAzoEMA and P*n*BMA was measured by ^{1}H NMR.

random copolymer block, it is more difficult to develop a directional interaction pair with PS. Thus, the effect of directional interactions could be ignored. Upon UV irradiation, all of the three disordered d_8-PS-*b*-P(*n*BMA-*r*-AzoEMA) BCPs were driven toward the LDOT due to a gain in entropy from the motions generated by the photoisomerization of azobenzene.

Experimental Section

Three d_8-PS-*b*-P(*n*BMA-*r*-AzoEMA) BCPs with MWs of M_n = 24 000, 40 000, and 47 000 (designated as Azo24k, Azo40k, and Azo47k, respectively) were synthesized through combining sequential anionic polymerization and postfunctionalization in a similar way reported previously.[27,48] Shown in Scheme 1 is the chemical structure of d_8-PS-*b*-P(*n*BMA-*r*-AzoEMA) BCPs. MWs and polydispersity indices (PDIs) of d_8-PS-*b*-P(*n*BMA-*r*-AzoEMA) BCPs were characterized by gel permeation chromatography (GPC) using a Knauer K-501 Pump with a K-2301 refractive index (RI) detector and a K-2600 UV detector and a column bank consisting of two Polymer Laboratories PLGel Mixed D columns and one PLGel 50 Å column (15 × 300 mm) in THF as eluent at a flow rate of 1.0 mL/min against linear polystyrene standards. Their compositions were determined by ^{1}H nuclear magnetic resonance (NMR) spectroscopy in $CDCl_3$ on Brüker Avance 400 (^{1}H) spectrometer with a Brüker BBO5 probe. Table 1 summarizes the characteristics of Azo24k, Azo40k, and Azo47k BCPs. As reported previously, T_gs of PnBMA and PAzoEMA are 25 °C[49] and 87 °C,[48] respectively. According to Fox equation of the glass transition, it is estimated that T_g of azobenzene-functionalized P(*n*BMA-*r*-AzoEMA) copolymers are around ~50 °C, well above room temperature.

Temperature-dependent SANS measurements were performed at the NG7 30 m SANS instrument at the National Institute of Standards and Technology in Gaithersburg, MD (see ref 50 for details of instrument design and operation) from 130 to 200 °C with an interval of 10 °C. The wavelength of neutrons, λ, is 6 Å with full width half-maximum $\Delta\lambda/\lambda = 0.11$. Three configurations were used: one with the detector offset by 20 cm and a sample−detector distance of 1 m, the second with a sample−detector distance of 4 m, and the third with a sample−detector distance of 13 m. The measured scattering intensity was corrected by instrument dark current, empty cell scattering, the sensitivity of individual detector pixels, and beam transmission. The absolute neutron scattering intensity was obtained by use of the available data reduction macros based on the Igor Pro data analysis package through the direct beam flux method.[51] To elicit the effective interaction parameter, χ_{eff}, SANS data in the absolute intensity were analyzed by the smeared random phase approximation (RPA) model for di-BCPs.[39,52−56] The coherent scattering intensity for di-BCPs in the disordered state $I(q)$ is related to the product of contrast factor and structure factor $S(q)$, which can be expressed as

$$I(q) = K(a-b)^2 S(q) \quad (1)$$

with

$$S(q) = \left[\frac{G(q)}{W(q)} - 2\chi_{eff}\right]^{-1} \quad (2)$$

where q is the magnitude of the scattering vector, K is a proportional constant, a and b are the coherent neutron scattering length densities, and χ_{eff} is the effective interaction parameter. In eq 2, $G(q)$ is the sum of Fourier transforms of the different density−density correlation functions in the system

$$G(q) = G_{AA}(q) + 2G_{AB}(q) + G_{BB}(q) \quad (3)$$

and $W(q)$ is the determinant of these same terms

$$W(q) = G_{AA}(q)G_{BB}(q) - \{G_{AB}(q)\}^2 \quad (4)$$

$G_{AA}(q)$, $G_{BB}(q)$, and $G_{AB}(q)$ in eqs 3 and 4 are the generalized correlation functions for a melt of polydisperse Gaussian A-*b*-B or A-*b*-C_xD_{1-x} di-BCP coils with unequal Kuhn lengths of two segment types (the detailed expressions are given in the Supporting Information). The incoherent scattering intensity was set as one of the fitting parameters and was corrected for the fitting results.

Bulk samples for the SANS measurements were prepared by compression-molding Azo24k, Azo40k, and Azo47k BCPs into 1.5 cm diameter disks with ~0.8 mm thickness at 130 °C. The disks were then annealed at 130 °C under vacuum for 72 h. Samples for SANS measurements were placed into demountable titanium cells fitted with quartz windows. The entire assembly was mounted on a remote-controlled multisampling block with a heating setup designed for the neutron spectrometer. Prior to each measurement, the samples were allowed 30 min to achieve thermal equilibrium. The temperature was monitored and controlled by a thermocouple located in close proximity to the samples. The temperature control was within ±1 °C at each temperature.

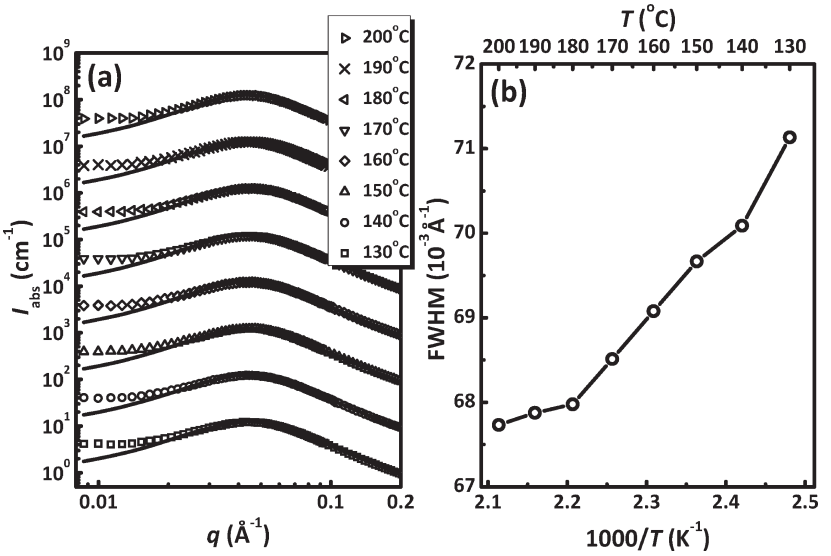

Figure 1. (a) SANS profiles (open symbols) and the smeared RPA calculations (solid lines) of the Azo24k BCP at different temperatures ranging from 130 to 200 °C with an interval of 10 °C. Note: the profiles have been shifted vertically by a factor of 10 for clarity. (b) The corresponding fwhm of correlation-hole scattering maximum as a function of temperature.

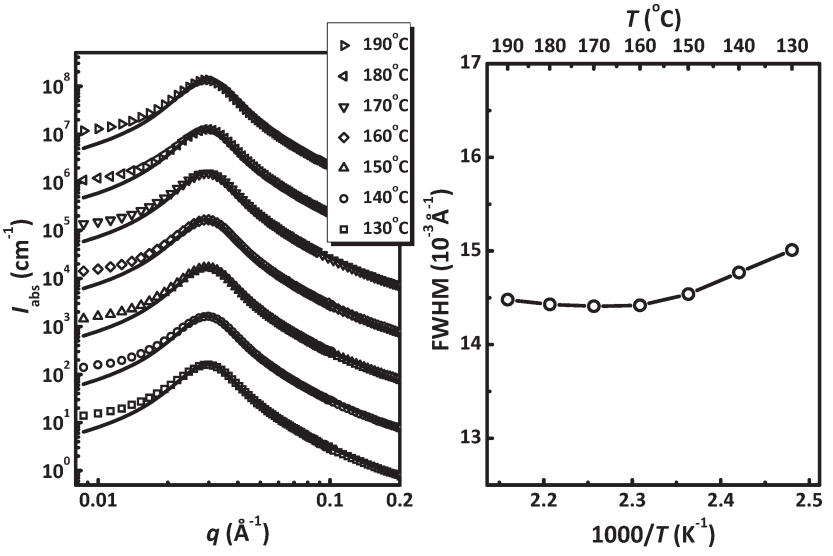

Figure 2. (a) Temperature-dependent SANS profiles (open symbols) and the smeared RPA calculations (solid lines) for the Azo47k BCP in the range from 130 to 190 °C with an interval of 10 °C. Note: the profiles have been shifted vertically by a factor of 10 for clarity. (b) Corresponding fwhm of the correlation-hole scattering maximum as a function of temperature.

A Newport's Oriel light source equipped with a high-power mercury arc lamp (500 W), a digital light intensity controller, and a 365 nm wavelength filters was used for investigating the photoresponses of these d_8-PS-*b*-P(*n*BMA-*r*-AzoEMA) BCPs in films. Toluene solutions of Azo24k, Azo40k, and Azo47k BCPs were spin-coated onto silicon wafers, forming the films with a thickness of ~800 nm. After annealing at 180 °C under vacuum for 48 h, these films were cut into two pieces with the same shape and size. One was kept in the dark; the other was exposed to UV light with a wavelength of 365 nm and an intensity of 35 mW/cm^2 for 1 h at 180 °C under N_2. After UV treatments, the thin film was quenched to low temperature using liquid nitrogen. SANS measurements were performed on them at room temperature, and the incident neutron beam was perpendicular to the films and repeated on the same instrument in two different beamtimes.

Results and Discussion

Figures 1a, 2a, and 3a show a series of SANS profiles (the absolute scattering intensity $I_{abs}(q)$ vs q, where q is the scattering vector given by $4\pi(\sin\theta)/\lambda$ with 2θ and λ denoting scattering angle and wavelength) of Azo24k, Azo47k, and Azo40k BCPs, respectively, at temperatures from 130 to 200 °C. In all the scattering profiles, a broad and diffuse maximum arising from the correlation hole scattering was observed, indicating that the three BCPs are all in a disordered state over the entire temperature range. The corresponding full widths at half-maximum (fwhm) of the correlation hole scattering maxima, which are determined by a smeared Lorentzian fit, as a function of the inversed temperatures are given in Figures 1b, 2b, and 3b. For Azo24k BCP, the fwhm continuously increases with the inversed temperature, similar to the trend observed in their parent PS-*b*-P*n*BMA BCPs. In fact, this is typical for a disordered BCP with a LDOT-type phase behavior. For Azo47k BCP, the fwhm is almost temperature-independent. For Azo40k BCP, a gradual decrease of the fwhm with increasing the inversed temperature corresponds to a UODT-type phase behavior of BCPs.

To elicit the empirical Flory−Huggins segmental interaction parameter, χ_{eff}, we compared the calculated scattering profiles by

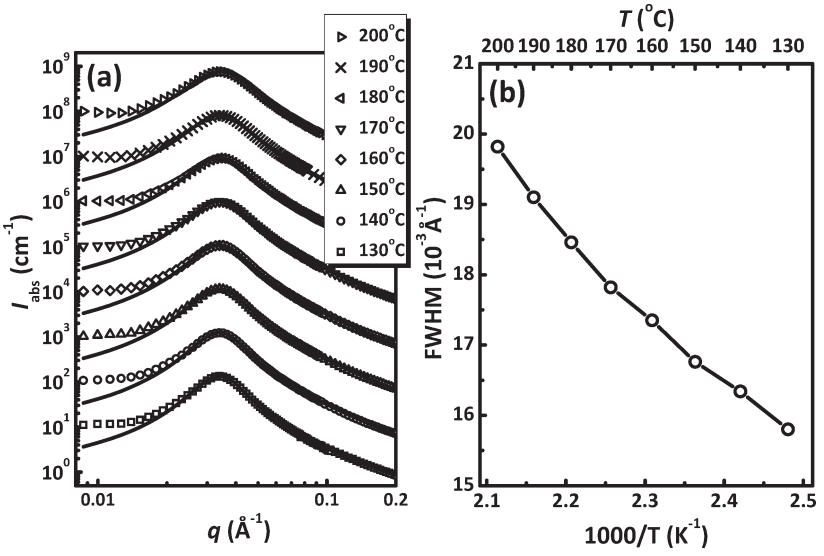

Figure 3. (a) Temperature-dependent SANS profiles (open symbols) and the smeared RPA calculations (solid lines) for the Azo40k BCP in the range from 130 to 200 °C with an interval of 10 °C. Note: the profiles have been shifted vertically by a factor of 10 for clarity. (b) Corresponding fwhm of the correlation-hole scattering maximum as a function of the inversed temperatures.

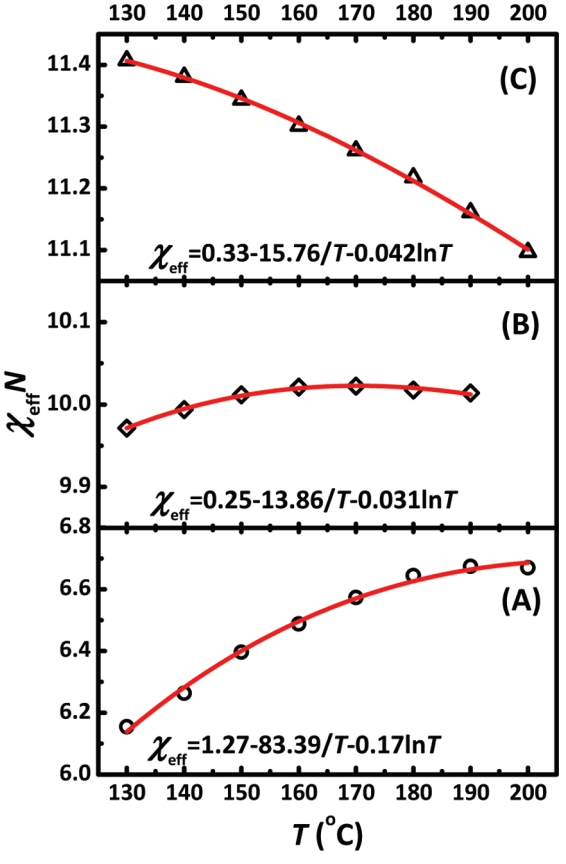

Figure 4. Temperature dependence of $\chi_{eff}N$ extracted from SANS data of Azo24k (A), Azo47k (B), Azo40k (C) BCPs by a smeared RPA calculation for binary mixtures of di-BCPs.

use of the compressible RPA model for di-BCPs on the basis of the modified Leibler's scattering function $S(q)$ to the experimental data $I_{abs}(q)$.[43,52,56−59] The representative calculated SANS profiles of Azo24k, Azo47k, and Azo40k BCPs are indicated by solid lines in Figures 1a, 2a, and 3a, respectively, and the extracted χ_{eff} of Azo24k, Azo47k, and Azo40k BCPs at each temperature is shown in Figure 4. It is evident that the agreement between the calculations and the experimental data is fairly good over the entire scattering vector range, except for those data points at very small q ($q \leq 0.02$ Å^{-1}). This disagreement may come from the approximation of the finite compressibility, in which the compressible BCP melt is modeled by treating the free volume as nonselective solvent molecules in an incompressible-solvent system (see the Supporting Information for more details). As expected, the temperature dependence of χ_{eff} for Azo24k, Azo47k, and Azo40k BCPs exhibits a similar trend in the fwhm as a function of the inversed temperatures. For Azo24k BCP, $\chi_{eff}N$ increases from 6.155 to 6.670 as temperature increases from 130 to 200 °C; for Azo47k BCP, $\chi_{eff}N$ nearly keeps constant (~10) within the experimental temperature range; for Azo40k BCP, $\chi_{eff}N$ gradually decreases from 11.408 to 11.161 as temperature increases. All these observed phenomena are similar to the general behaviors of their parent PS-*b*-P*n*BMA BCPs. PS-*b*-P*n*BMA BCP melts are well-known to exhibit an hourglass-shaped phase diagram, resulting from the simultaneous appearance of a UDOT and a LDOT, in accordance with numerous experimental observations[30−35] and compressible RPA calculations.[29,36−46] More intriguing, Yeung et al., who combined equation-of-state theory with standard descriptions of the order-to-disorder transition (ODT) in di-BCPs, have theoretically predicted the temperature dependence of $\chi_{eff}N$. Upon heating, $\chi_{eff}N$ increases when the PS-*b*-P*n*BMA BCP is close to LDOT, whereas $\chi_{eff}N$ decreases when the PS-*b*-P*n*BMA BCP is close to UODT. In the intermediate region between UODT and LDOT, $\chi_{eff}N$ is almost temperature-independent. Similarly, it can be anticipated that Azo24k and Azo40k BCPs are closer to LDOT and UODT, respectively, whereas Azo47k BCP locates in the intermediate region between UODT and LDOT. Consequently, d_8-PS-*b*-P(*n*BMA-*r*-AzoEMA) BCPs still remain the "compressible" nature of their parent PS-*b*-P*n*BMA BCPs.

Conventionally, the experimental χ_{eff} is simply expressed as $\chi_{eff} = A + B/T$ in the absolute temperature (K) for di-BCPs.[15] For the LDOT systems, however, a more general expression $\chi_{eff} = A/T + B \ln T + C$, where A, B, and C are constants, is used to represent the experimental χ_{eff}.[60] Using the latter expression, the following χ_{eff} are determined: $\chi_{eff} = 1.27 - 83.39/T - 0.17 \ln T$ for Azo24k BCP; $\chi_{eff} = 0.25 - 13.86/T - 0.031 \ln T$ for Azo47k BCP, and $\chi_{eff} = 0.33 - 15.76/T - 0.042 \ln T$ for Azo40k BCPs. This indicates that the phase behavior of d_8-PS-*b*-P(*n*BMA-*r*-AzoEMA) BCPs highly depend on the temperature-dependent χ_{eff}. Furthermore, as can be seen, χ_{eff} of Azo24k BCP is comparable to that of PS-*b*-P*n*BMA BCP with a MW of M_n = 47 200,

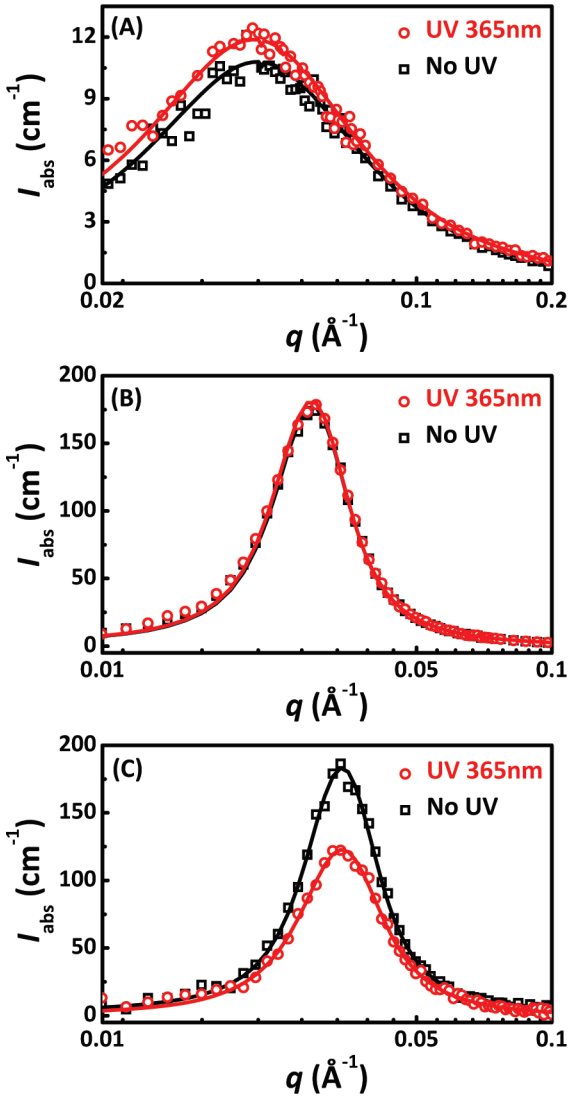

Figure 5. SANS profiles (open symbols) and the corresponding smeared RPA calculations (solid lines) for Azo24k (A), Azo47k (B), and Azo40k (C) BCPs before (black) and after (red) exposure to UV light with a wavelength of 365 nm and an intensity of 35 mW/cm^2 for 1 h at 180 °C under N_2.

which is close to LDOT ($\chi_{eff} = 0.97 - 64.21/T - 0.13 \ln T$),[34] confirming that the integration of azobenzene functionalities does not change the general phase behavior of PS-*b*-P*n*BMA BCPs. In addition, the χ_{eff} of three d_8-PS-*b*-P(*n*BMA-*r*-AzoEMA) BCPs are very sensitive to the MW and composition of the copolymers, that is, the "chemistry" characteristics of BCPs. Currently, the influence of chemical details on the phase behaviors of BCPs still remain to be interpreted both experimentally and theoretically.

The photoresponses of three d_8-PS-*b*-P(*n*BMA-*r*-AzoEMA) BCPs were investigated by SANS in BCP films (Figure 5). The SANS profiles for three BCP films exhibit a single, broad correlation hole scattering maximum, identical to the corresponding SANS results of their copolymer melts. After irradiation with 365 nm UV light, the absolute intensity of correlation-hole scattering, $I_{max}(q)$, shows different types of responses from these BCP films. For Azo24k BCP, $I_{max}(q)$ increases; for Azo 47k BCP, $I_{max}(q)$ keeps constant; for Azo40k BCP, $I_{max}(q)$ decreases. By fitting $I_{abs}(q)$ to the above-described RPA model, the changes of $\chi_{eff}N$ upon exposure to UV light were extracted. For Azo24k BCP, $\chi_{eff}N$ increases from 5.187 to 5.280. For Azo47k BCP, $\chi_{eff}N$ almost keeps unchanged (10.070 without UV irradiation and 10.076 after UV exposure). For Azo40k, $\chi_{eff}N$ decreases from 11.400 to 11.383. Clearly, UV irradiation has a similar effect to temperature on the PS-*b*-P(*n*BMA-*r*-AzoEMA) BCPs: increasing temperature drives the disordered BCPs toward LDOT, so does UV irradiation. Such photoresponses originate from the motions generated by the photoisomerization of azobenzene, leading to a significant increase in entropy as a result of conformational increase and density variation. As shown in our previous studies,[27] however, the yield of azobenzene photoisomerization in BCP thin films, in comparison with those previously reported azobenzene-containing polymers, would be still low due to the thermo-induced backward *cis*−*trans* isomerization. Consequently, only a weak driving force was generated upon UV irradiation.

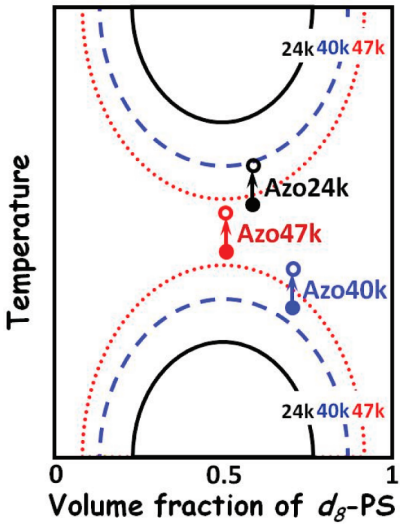

Figure 6. Schematic temperature−volume fraction diagram for Azo24k (A), Azo47k (B), and Azo40k (C) BCPs. Both UODT and LDOT for BCPs with different MWs are indicated by the black solid, blue dashed, and red dotted lines. The solid and empty spheres correspond to the state of three BCPs before and after UV exposure, respectively.

Conclusions

To summarize the phase behaviors and photoresponses of three d_8-PS-*b*-P(*n*BMA-*r*-AzoEMA) BCPs, a schematic temperature−volume fraction diagram for three P(*n*BMA-*r*-AzoEMA) BCPs is presented in Figure 6. Investigation of the phase behaviors has demonstrated that after randomly incorporating azobenzene functionalities into P*n*BMA blocks the d_8-PS-*b*-P(*n*BMA-*r*-AzoEMA) BCPs are still characteristic of the "compressibility", similar to the parent PS-*b*-P*n*BMA BCPs which exhibit both LDOT and UODT. Usually, the LDOT decreases as MWs increases. The UODT, on the other hand, increases with MWs.[30−32,34,40,61] Azo24k and Azo40k BCPs are closer to their corresponding LDOT and UODT, respectively, while Azo47k BCP locates in the middle of temperature interval between UODT and LDOT. Upon UV irradiation with a wavelength of 365 nm, the photoisomerization of azobenzene produces light-induced motions in the BCPs and thereby leads to conformational increase and density variation, which gives rise to a significant increase in entropy. Such an entropic gain drives the disordered d_8-PS-*b*-P(*n*BMA-*r*-AzoEMA) BCPs toward LDOT. Consequently, when a phase-mixed d_8-PS-*b*-P(*n*BMA-*r*-AzoEMA) BCP is very close to LDOT, UV exposure would bring about a photoinduced ordering transition from a homogeneous mixture to an ordered state with microdomains of each block. Considering the reversed *cis*−*trans* isomerization of

azobenzene induced by visible light, the reversible photocontrol over such an ordering process is quite promising. As mentioned in the Introduction, by applying the photocombing method via a reversibly photocontrollable ordering process comparable to the classic zone refinement, long-range ordered arrays of BCP microdomains could be created over a microscopic distance without touching samples. Moreover, it is well-known that PS-*b*-P*n*BMA BCP is also a representative baroplastic;[30−32,44,49] that is, the LDOT is very sensitive to pressure so that an ordered BCP can be transformed into a disordered state simply by applying hydrostatic pressure.[62−66] Most recently, this pressure-dependent property has been exploited for applications in data storage by using a scanning probe tip to apply a localized pressure.[67,68] Similarly, pressure may cause a local ODT for d_8-PS-*b*-P(*n*BMA-*r*-AzoEMA) BCPs, making it possible to revert UV-induced LDOT back. Accordingly, the combination of UV irradiation and applying local pressure would offer a novel way to reversibly control the LDOT in d_8-PS-*b*-P(*n*BMA-*r*-AzoEMA) BCPs.

Acknowledgment. This research was supported by the Department of Energy, Office of Basic Energy Science (DE-FG02-02ER45998), and the National Science Foundation-supported Material Research Science and Engineering Center (MRSEC) at the University of Massachusetts, Amherst (DMR-0213695). We thank Dr. B. Hammouda for the helpful discussions and Dr. Y. Liu for the assistance with SANS measurements. This work utilized facilities supported in part by the National Science Foundation under Agreement DMR-0454672. We acknowledge the support of the National Institute of Standards and Technology, U.S. Department of Commerce, in providing the neutron research facilities used in this work.

Supporting Information Available: RPA model for SANS analysis; segmental lengths and $\chi_{eff}N$ extracted from the smeared RPA fitting of SANS profiles. This material is available free of charge via the Internet at http://pubs.acs.org.

References and Notes

(1) Minko, S. *Responsive Polymer Materials: Design and Applications*; Wiley-Blackwell: Hoboken, NJ, 2006.
(2) Liu, F.; Urban, M. W. *Prog. Polym. Sci.* **2009**, *35*, 3–23.
(3) Huck, W. T. S. *Mater. Today* **2008**, *11*, 24–32.
(4) Yagai, S.; Kitamura, A. *Chem. Soc. Rev.* **2008**, *37*, 1520–1529.
(5) Dai, S.; Ravi, P.; Tam, K. C. *Soft Matter* **2009**, *5*, 2513–2533.
(6) Zhao, Y.; Ikeda, T. *Smart Light-Responsive Materials: Azobenzene-Containing Polymers and Liquid Crystals*; John Wiley & Sons, Inc.: Hoboken, NJ, 2009.
(7) Zhao, Y.; He, J. *Soft Matter* **2009**, *5*, 2686–2693.
(8) Sekkat, Z.; Knoll, W. *Photoreactive Organic Thin Films*; Academic Press: San Diego, 2002.
(9) Yin, R.; Xu, W.; Kondo, M.; Yen, C.-C.; Mamiya, J.-i.; Ikeda, T.; Yu, Y. *J. Mater. Chem.* **2009**, *19*, 3141–3143.
(10) Yamada, M.; Kondo, M.; Mamiya, J.-i.; Yu, Y.; Kinoshita, M.; Barrett, C. J.; Ikeda, T. *Angew. Chem., Int. Ed.* **2008**, *47*, 4986–4988.
(11) Seki, T.; Nagano, S. *Chem. Lett.* **2008**, *37*, 484–489.
(12) Natansohn, A.; Rochon, P. *Chem. Rev.* **2002**, *102*, 4139–4176.
(13) Tanchak, O. M.; Barrett, C. J. *Macromolecules* **2005**, *38*, 10566–10570.
(14) Yager, K. G.; Tanchak, O. M.; Godbout, C.; Fritzsche, H.; Barrett, C. J. *Macromolecules* **2006**, *39*, 9311–9319.
(15) Hamley, I. W. *The Physics of Block Copolymers*; Oxford University Press: New York, 1998.
(16) Hadjichristidis, N.; Pispas, S.; Floudas, G. *Block Copolymers: Synthetic Strategies, Physical Properties, and Applications*; John Wiley & Sons: New York, 2002.
(17) Bang, J.; Jeong, U.; Ryu, D. Y.; Russell, T. P.; Hawker, C. J. *Adv. Mater.* **2009**, *21*, 4769–4792.
(18) Ross, C. A.; Cheng, J. Y. *MRS Bull.* **2008**, *33*, 838–845.
(19) Hawker, C. J.; Russell, T. P. *MRS Bull.* **2005**, *30*, 952–966.
(20) Li, M.; Coenjarts, C. A.; Ober, C. K. *Adv. Polym. Sci.* **2005**, *190*, 183–226.
(21) Segalman, R. A. *Mater. Sci. Eng.* **2005**, *R48*, 191–226.
(22) Kadota, S.; Aoki, K.; Nagano, S.; Seki, T. *J. Am. Chem. Soc.* **2005**, *127*, 8266–8267.
(23) Morikawa, Y.; Nagano, S.; Watanabe, K.; Kamata, K.; Iyoda, T.; Seki, T. *Adv. Mater.* **2006**, *18*, 883–886.
(24) Yu, H.; Iyoda, T.; Ikeda, T. *J. Am. Chem. Soc.* **2006**, *128*, 11010–11011.
(25) Travasso, R. D. M.; Kuksenok, O.; Balazs, A. C. *Langmuir* **2005**, *21*, 10912–10915.
(26) Travasso, R. D. M.; Kuksenok, O.; Balazs, A. C. *Langmuir* **2006**, *22*, 2620–2628.
(27) Chen, W.; Wang, J.-Y.; Wei, X.; Xu, J.; Balazs, A. C.; Matyjaszewski, K.; Russell, T. P. *Macromolecules* **2010**, in press.
(28) Huang, C.-F.; Chen, W.; Russell, T. P.; Balazs, A. C.; Chang, F.-C.; Matyjaszewski, K. *Macromol. Chem. Phys.* **2009**, *210*, 1484–1492.
(29) McMullen, W. E.; Freed, K. F. *Macromolecules* **1990**, *23*, 255–262.
(30) Russell, T. P.; Karis, T. E.; Gallot, Y.; Mayes, A. M. *Nature* **1994**, *368*, 729–731.
(31) Karis, T. E.; Russell, T. P.; Gallot, Y.; Mayes, A. M. *Macromolecules* **1995**, *28*, 1129–1134.
(32) Ruzette, A. V. G.; Banerjee, P.; Mayes, A. M.; Pollard, M.; Russell, T. P.; Jerome, R.; Slawecki, T.; Hjelm, R.; Thiyagarajan, P. *Macromolecules* **1998**, *31*, 8509–8516.
(33) Ruzette, A.-V. G. Molecular design of ordering transitions in block copolymers. Dissertation, Massachusetts Institute of Technology, Cambridge, MA, 2000.
(34) Ryu, D. Y.; Shin, C.; Cho, J.; Lee, D. H.; Kim, J. K.; Lavery, K. A.; Russell, T. P. *Macromolecules* **2007**, *40*, 7644–7655.
(35) Hammouda, B.; Bauer, B. J.; Russell, T. P. *Macromolecules* **1994**, *27*, 2357–2359.
(36) Dudowicz, J.; Freed, K. F. *Macromolecules* **1993**, *26*, 213–220.
(37) Tang, H.; Freed, K. F. *Macromolecules* **1991**, *24*, 958–966.
(38) Yeung, C.; Desai, R. C.; Shi, A.-C.; Noolandi, J. *Phys. Rev. Lett.* **1994**, *72*, 1834–1837.
(39) Bidkar, U. R.; Sanchez, I. C. *Macromolecules* **1995**, *28*, 3963–3972.
(40) Hino, T.; Prausnitz, J. M. *Macromolecules* **1998**, *31*, 2636–2648.
(41) Weidisch, R.; Stamm, M.; Schubert, D. W.; Arnold, M.; Budde, H.; Horing, S. *Macromolecules* **1999**, *32*, 3405–3411.
(42) Cho, J. *Macromolecules* **2000**, *33*, 2228–2241.
(43) Dudowicz, J.; Freed, K. F. *Macromolecules* **2000**, *33*, 5292–5299.
(44) Ruzette, A. V. G.; Banerjee, P.; Mayes, A. M.; Russell, T. P. *J. Chem. Phys.* **2001**, *114*, 8205–8209.
(45) Cho, J. *Macromolecules* **2001**, *34*, 1001–1012.
(46) Cho, J. *Macromolecules* **2004**, *37*, 10101–10108.
(47) Cho, J. *J. Chem. Phys.* **2004**, *120*, 9831–9840.
(48) Breiner, T.; Kreger, K.; Hagen, R.; Hackel, M.; Kador, L.; Muller, A. H. E.; Kramer, E. J.; Schmidt, H.-W. *Macromolecules* **2007**, *40*, 2100–2108.
(49) Gonzalez-Leon, J. A.; Acar, M. H.; Ryu, S.-W.; Ruzette, A.-V. G.; Mayes, A. M. *Nature* **2003**, *426*, 424–428.
(50) Glinka, C. J.; Barker, J. G.; Hammouda, B.; Krueger, S.; Moyer, J. J.; Orts, W. J. *J. Appl. Crystallogr.* **1998**, *31*, 430–445.
(51) Kline, S. R. *J. Appl. Crystallogr.* **2006**, *39*, 895–900.
(52) Leibler, L. *Macromolecules* **1980**, *13*, 1602–1617.
(53) Bates, F. S.; Hartney, M. A. *Macromolecules* **1985**, *18*, 2478–2486.
(54) Benoit, H.; Hadziioannou, G. *Macromolecules* **1988**, *21*, 1449–1464.
(55) Hashimoto, T.; Koizumi, S.; Hasegawa, H. *Macromolecules* **1994**, *27*, 1562–1570.
(56) Sakurai, S.; Nomura, S. *Polymer* **1997**, *38*, 4103–4112.
(57) Fredrickson, G. H.; Helfand, E. *J. Chem. Phys.* **1987**, *87*, 697–705.
(58) Bates, F. S.; Rosedale, J. H.; Fredrickson, G. H.; Glinka, C. J. *Phys. Rev. Lett.* **1988**, *61*, 2229–2232.
(59) Bates, F., S.; Rosedale, J. H.; Fredrickson, G. H. *J. Chem. Phys.* **1990**, *92*, 6255–6270.
(60) Qian, C.; Mumby, S. J.; Eichinger, B. E. *Macromolecules* **1991**, *24*, 1655–1661.
(61) Ryu, D. Y.; Jeong, U.; Kim, J. K.; Russell, T. P. *Nature Mater.* **2002**, *1*, 114–117.
(62) Pollard, M.; Russell, T. P.; Ruzette, A. V.; Mayes, A. M.; Gallot, Y. *Macromolecules* **1998**, *31*, 6493–6498.
(63) Pollard, M. A. The Disorder-to-Order Phase Transition in Poly(Styrene-block-n-Butyl Methacrylate): the Effect of Pressure.

Dissertation, University of Massachusets—Amherst, Amherst, MA, 2001.
(64) Ruzette, A. V. G.; Mayes, A. M.; Pollard, M.; Russell, T. P.; Hammouda, B. *Macromolecules* **2003**, *36*, 3351–3356.
(65) Ryu, D. Y.; Lee, D. J.; Kim, J. K.; Lavery, K. A.; Russell, T. P.; Han, Y. S.; Seong, B. S.; Lee, C. H.; Thiyagarajan, P. *Phys. Rev. Lett*. **2003**, *90*, 235501.
(66) Lavery, K. A. Pressure effects on entropically driven phase transitions in block copolymers. Dissertation, University of Massachusetts—Amherst, Amherst, MA, 2005.
(67) Russell, T. P.; Lee, D. H. *Nature Nanotechnol*. **2009**, *4*, 703–704.
(68) Jo, A.; Joo, W.; Jin, W.-H.; Nam, H.; Kim, J. K. *Nature Nanotechnol*. **2009**, *4*, 727–731.